ISIJ International, Vol. 46 (2006), No. 3, pp. 420–426

Thermal Conductivity of the $CaO–Al_2O_3–SiO_2$ System

Youngjo KANG and Kazuki MORITA

Department of Materials Engineering, University of Tokyo, Tokyo 113-8656 Japan. E-mail: kzmorita@iis.u-tokyo.ac.jp

(*Received on September 8, 2005; accepted on November 1, 2005*)

Thermal conductivity of the $CaO–Al_2O_3–SiO_2$ system, which is one of the most important silicate melts in iron- and steelmaking processes, was measured using non-stationary hot wire method in the range from liquidus temperature to 1 873 K. Measurements were carried out at various compositions, and iso-thermal conductivity line of the $CaO–Al_2O_3–SiO_2$ system was drawn in iso-thermal sections at 1 673 K, 1 773 K, and 1 873 K. Thermal conductivity decreased with basicity increase, when CaO/SiO_2 ratio is smaller than unity, whereas it showed constant value when CaO/SiO_2 ratio is larger. In case Al_2O_3 content was varied at constant CaO/SiO_2 ratio of 0.39 and 0.90, thermal conductivity showed maximum at 15–20 mass% Al_2O_3, suggesting that Al_2O_3 behaves as an amphoteric oxide. In the temperature range of interest, the thermal conductivity of each composition decreased as temperature rises. Temperature dependence showed deviation from linearity with the reciprocal of absolute temperature, which was considered to be due to the thermally-induced depolymerisation of the silicate structure at higher temperature. Also, thermal conductivity was found to conform to an exponential function of $1/T$ during deployerization with the apparent activation energy.

KEY WORDS: thermal conductivity; slag; non-stationary hot wire method; silicate melt; IR.

1. Introduction

Most of processes in iron- and steelmaking at high temperature involve heat transfer phenomena, and thermal properties such as thermal conductivities of slags and fluxes are very important to improve each process and the product quality. Accordingly, accurate thermal conductivity data of silicate melts have been strongly required. For instance, thermal conductivity of mould powders has been intensively investigated, because the surface quality of final product may be governed by heat transfer through mould flux.[1] Nagata *et al.*[2–5] have measured the thermal conductivity of the $Na_2O–SiO_2$ binary system the using non-stationary hot wire method, and they showed that the thermal conductivity of alkali silicate had the linear relationship with the reciprocal of absolute temperature.[4]

While many environmental issues become more noteworthy, most of the blast furnace slag is recycled for various applications among which more than 60% is BF slag cement.[6] Morphology of BF slags, such as degree of crystallization, granular size, *etc.*, affect the properties of the recycled products and it can be attained only under well-controlled heat transfer.[7] Also, utilization of intrinsic heat of molten slag has been proposed by Akiyama *et al.*,[8] which would lead to a significant reduction of CO_2 generation even by applying to the calcination of limestone for BF slag cement.

However, thermal conductivity data of the $CaO–Al_2O_3–SiO_2$ system, a typical system of BF slags, have not been clarified enough over a wide range of composition. As shown in **Table 1**, there are several data measured at temperatures lower than 1 773 K. Recently, thermal diffusivity of the $CaO–Al_2O_3–SiO_2$ system has been investigated using laser flash method by Seetharaman *et al.*[15] They have studied the effect of composition on the thermal diffusivity and the structure of the $CaO–Al_2O_3–SiO_2$ system, but the effect of temperature on thermal properties and structure was not considered. Difficulties on thermal conductivity measurement are often caused by convection and radiation at high temperature above melting point. Non-steady methods may be advantageous rather than steady ones due to the shorter measurement periods.[16] Furthermore, it is well known that the thermal conductivity measured by laser flash method may involve larger contribution of radiation,[17] compared with the hot wire method.

In the present study, measurements of the thermal conductivity with respect to various compositions of the $CaO–Al_2O_3–SiO_2$ system were carried out at temperature ranging from 1 673 to 1 873 K using the hot wire method. Another objective is to clarify the relationship between thermal conductivity and structure of silicate melts based on the investigation of their composition and temperature dependencies of the thermal conductivity.

2. Experimental

2.1. Theory and Measurement Procedures

In the present study, non-stationary hot wire method is employed for the measurement of thermal conductivity of silicate melts. From the one solution of heat transfer equation, thermal conductivity, λ (W/m K), can be obtained as Eq. (1).[18]

Table 1. Reported values of thermal conductivity for the $CaO–Al_2O_3–SiO_2$ system.

COMPOSITION (mass%)	METHOD	TEMPERATURE RANGE (K)	THERMAL CONDUCTIVITY (W/mK)	AUTHOR	REF.
40%CaO-20%Al_2O_3-40%SiO_2	hot wire method	373~1673	0.20~1.50	Nagata *et al.*	2)
25%CaO-15%Al_2O_3-60%SiO_2		373~1673	0.40~1.60	Nagata *et al.*	2)
40%CaO-20%Al_2O_3-40%SiO_2		1573	0.80~1.00	Ishikuro *et al*	9)
40%CaO-20%Al_2O_3-40%SiO_2		373~1673	0.50~1.70	Nagata *et al.*	3)
40%CaO-20%Al_2O_3-40%SiO_2	laser flash method	273~1623	0.70~1.20	Kishimoto *et al.*	10)
45%CaO-15%Al_2O_3-40%SiO_2		273~1673	0.60~1.20	Kishimoto *et al.*	10)
50%CaO-15%Al_2O_3-35%SiO_2		273~1673	0.50~1.00	Kishimoto *et al.*	10)
50%CaO-15%Al_2O_3-35%SiO_2		1273~1723	0.50	Sakuraya *et al.*	11)
35%CaO-20%Al_2O_3-45%SiO_2		1273~1723	0.70~0.80	Sakuraya *et al.*	11)
40%CaO-20%Al_2O_3-40%SiO_2	RHF	1573~1623	1.10~2.00	Ogino *et al.*	12)
40%CaO-20%Al_2O_3-40%SiO_2		1273~1673	1.00~2.00	El Gammal *et al.*	13)
CaO-Al_2O_3-SiO_2 system		m.p.+100	0.70~2.80	Sommerville *et al.*	14)

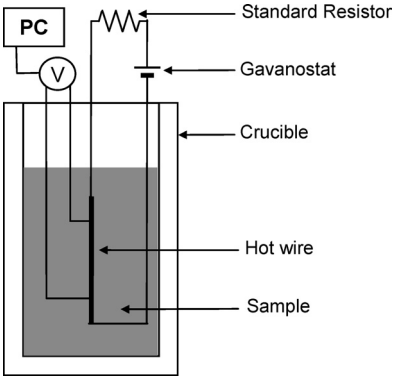

Fig. 1. Schematic diagram of measurement setup of the hot wire method.

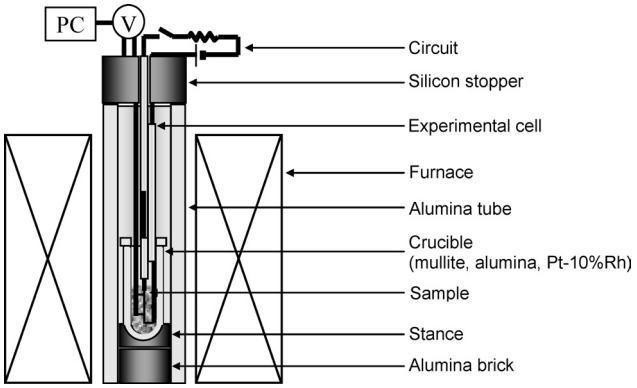

Fig. 2. Schematic representation of the experimental apparatus.

$$\lambda = \frac{Q}{4\pi} \Big/ \frac{d\Delta T}{d \ln t} \quad \text{.....(1)}$$

Here, Q (W/m) denotes the heat generation rate of hot wire per unit length. The thermal conductivity of sample can be obtained from Q and the slope of ΔT (K) *versus* $\ln t$.

Figure 1 shows the schematic diagram of apparatus for the hot wire method, where 0.15 mmϕ Pt–13%Rh wire plays a role of thermocouple as well as heating element. The circuit for thermal conductivity measurement consists of hot wire, Galvanostat, 10 mΩ standard resistor and 0.5 mmϕ Pt wire. Supplying a constant electric power with about 1.5 A to hot wire immerged into the center of sample, the voltage change of hot wire between 2 terminals was monitored for no longer than 30 s. From stored data in PC, a curve of ΔV *versus* $\ln t$ was plotted. Since the voltage change deviates from linearity presumably due to the convection, the linear range should be determined by differentiating the curve and the slope of the straight line was evaluated. Obtained slope can be converted to that of ΔT *versus* $\ln t$ using the following relationships.

$$V = I \cdot R = I \cdot R_{273} \cdot f(T) = I \cdot R_{273} \cdot \{a(T-273)^2 + b(T-273) + 1)\} \quad \text{.....(2)}$$

Here, R_{273} denotes the resistance of wire at 273 K and $f(T)$ does the temperature coefficient of resistance.[19] In case of Pt–13%Rh wire, the constants a and b were estimated from the curve of the wire resistance against temperature as -1.44×10^{-7} and 1.56×10^{-3}.

The apparatus used in the measurement are illustrated in **Fig. 2**. The $CaO–Al_2O_3–SiO_2$ oxide sample was held in an alumina tanmann tube or a manufactured Pt–10%Rh crucible with inner diameter of 32 mm to avoid significant composition change by Al_2O_3 dissolution. Sample filled in a holder was set in an electric resistance furnace with the heating element of $MoSi_2$. The upper level of sample was adjusted to the highest temperature zone in order to eliminate free convection during the measurement. The thermal conductivity measurement was carried out at every 50 K in the temperature range from 1 573 K (or around each liquidus temperature) to 1 873 K.

After each measurement, samples for chemical analysis were taken and the chemical compositions were determined by gravimetric analysis for Si and ICP-AES for Al and Ca. For some samples, the structure of selected silicate melt was investigated by IR absorption spectroscopy. Selected samples were quenched in air, and 0.2 mg of each sample was well-ground and mixed with 200 mg of KBr, and then pressed into a pellet with the diameter of 8 mm. A spectral resolution was set as 4 cm^{-1}, and data of 64 scans were averaged.

2.2. Sample Preparation

Samples for measurement were prepared by mixing reagent grade SiO_2, Al_2O_3 and CaO calcined from $CaCO_3$. Measurement compositions are represented in **Table 2** and

Table 2. Result of chemical analysis and measurement conditions.

Charge composition (mass%)			Analysed composition (mass%)			$\frac{CaO}{SiO_2}$	Liquidus Temperature (K)	Measurement Temperature (K)
CaO	Al_2O_3	SiO_2	CaO	Al_2O_3	SiO_2			
11.0	11.0	78.0	11.0±0	11.0±1	78.0±0	0.14	1773	1773~1873
26.0	8.0	66.0	22.0±1	9.0±1	65.5±1	0.39	1673	1723~1873
24.0	15.0	61.0	24.0±0	15.5±0	60.0±1	0.39	1443	1573~1873
22.0	22.0	56.0	25.0±1	22.0±1	55.0±1	0.39	1673	1673~1873
47.5	0.0	52.5	47.0±0	1.0±1	53.0±1	0.90	1810	1823~1873
30.0	18.0	52.0	28.0±1	22.0±2	50.0±2	0.58	1673	1573~1873
42.0	11.5	46.5	28.0±1	19.0±1	43.0±1	0.90	1673	1673~1873
26.0	30.0	44.0	24.5±1	30.0±1	45.0±1	0.58	1773	1773~1873
38.0	20.0	42.0	36.5±1	21.0±1	42.5±1	0.90	1538	1623~1873
29.0	39.0	32.0	38.0±1	40.0±2	32.0±2	0.90	1673	1673~1873
45.0	45.0	10.0	40.5±1	45.5±1	10.0±0	4.50	1723	1723~1773
40.5	50.5	9.0	45.0±1	50.5±1	9.0±0	4.50	1773	1773~1873

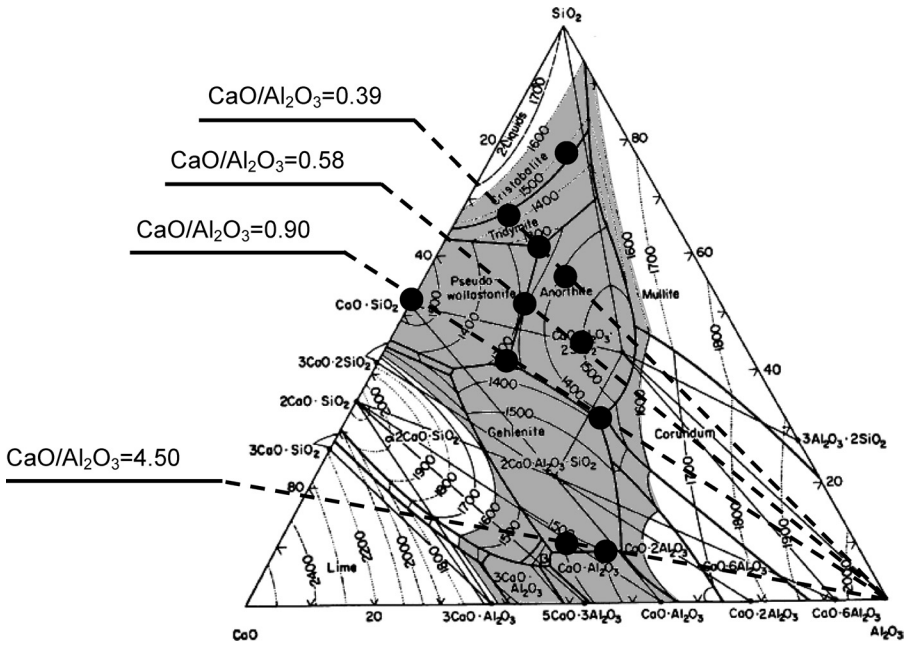

Fig. 3. Liquid region and measurement compositions in the iso-thermal cross section of the $CaO–Al_2O_3–SiO_2$ ternary system at 1 873 K.

in the ternary isothermal cross section of the $CaO–Al_2O_3–SiO_2$ system[20] as shown **Fig. 3**. And CaO/Al_2O_3 ratio was fixed to several values. Powder mixture filled in platinum crucible was premelted in the kanthal furnace at 1 773 K for 20 min. After quenching, pre-melted samples were prepared by crushing finely.

3. Result and Discussion

Measured thermal conductivities of the $CaO–Al_2O_3–SiO_2$ system with various compositions are plotted as a function of temperature in **Fig. 4**. Each composition is expressed in weight percent and distinguished by different symbols. All results were obtained from the measurements above respective liquidus temperatures. They show a good agreement with reported thermal conductivity data of similar compositions.[2]

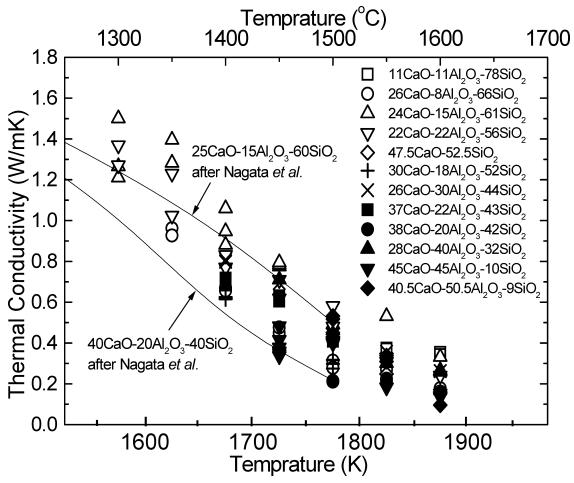

Fig. 4. Temperature dependence of thermal conductivity of the $CaO–Al_2O_3–SiO_2$ system.

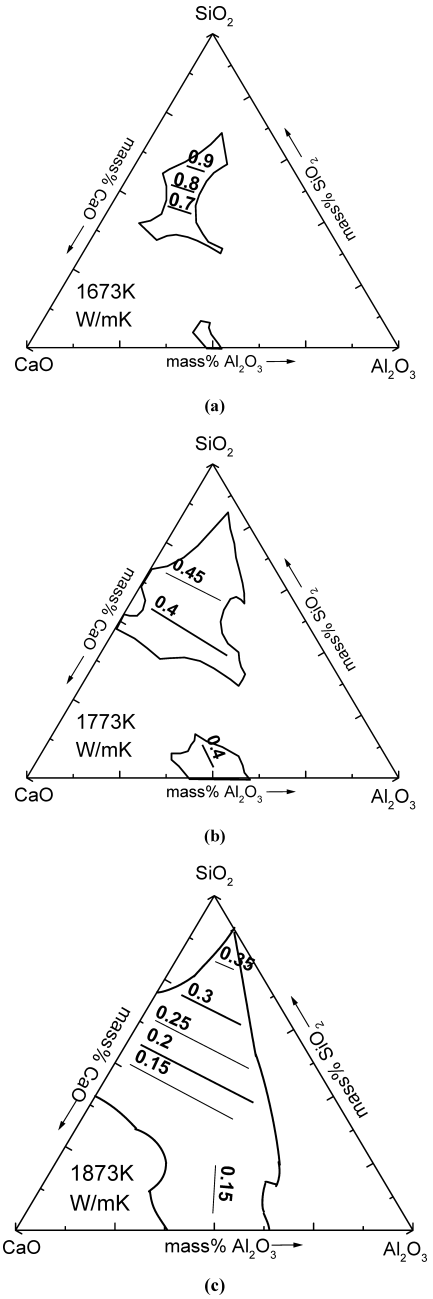

Fig. 5. Iso-thermal conductivity contours for the CaO–Al_2O_3–SiO_2 system at (a) 1 673 K, (b) 1 773 K and (c) 1 873 K.

Although these temperature dependences show slightly different behavior, a drastic decrease appears just above the liquidus temperature of every oxide composition. Thermal conductivity of the oxide shows higher values with increasing silica content at a certain temperature.

3.1. Composition Dependence

Thermal conductivities of the CaO–Al_2O_3–SiO_2 system are represented in its iso-thermal sections at 1 673 K, 1 773 K and 1 873 K as shown in **Figs. 5**(a), 5(b) and 5(c). As was previously mentioned, they show smaller values at the higher temperature and increase with basicity decrease. Composition dependence of the thermal conductivity measured in the present was explicitly clarified.

As is well known, heat is transferred mainly by lattice conduction, and this conduction is carried out through lattice vibration with a specific mode, so-called phonon. The thermal conduction in silicate melt is considered to depend strongly on this structure. Since acidic oxide, such as SiO_2, forms network with strong covalent bond in the silicate melt, while basic oxide breaks Si–O covalent bond to form ionic bond with cations, the present result indicates that the thermal conduction in silicate melt would occur effectively through covalent bond rather than ionic bond. This result is consistent with those by previous researchers.[5,21]

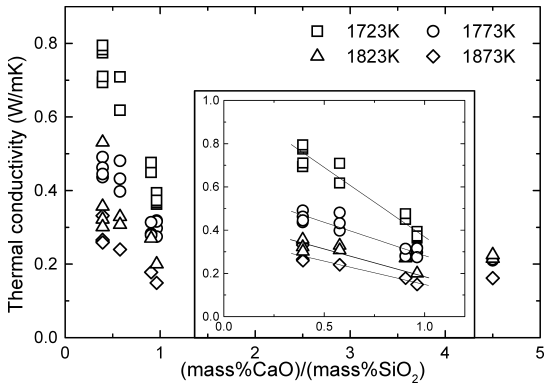

Fig. 6. Relationship between thermal conductivity and CaO/SiO_2 ratio.

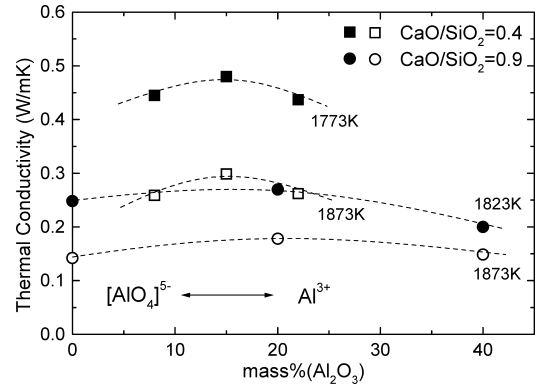

Fig. 7. Dependence of thermal conductivity of the CaO–Al_2O_3–SiO_2 system on Al_2O_3 content at constant CaO/SiO_2 ratios of 0.4 and 0.9.

Effect of basicity, the CaO/SiO_2 ratio, on the thermal conductivity of silicate melt is represented in **Fig. 6**. As basicity increases, thermal conductivity shows a drastic decrease, which is caused by the reduction in the number of covalent bonds in the melt. At CaO/SiO_2=4.5, however, thermal conductivity did not show such a small value as expected from the decrease in acidic region. This may be due to the saturation of non-bridging oxygen as well as the effect of amphoteric oxide Al_2O_3. The effect of Al_2O_3 was investigated at fixed CaO/SiO_2 ratios of 0.4, 0.6, 0.9 and 4.5. **Figure 7** shows the dependences of thermal conductivity on alumina content at CaO/SiO_2 ratios of 0.39 and 0.90. At low Al_2O_3 content region, the thermal conductivity increased as Al_2O_3 content increased. On the other hand, further addition of Al_2O_3 reduced the thermal conductivity, and the maximum value appeared at around 15–20 mass% Al_2O_3.

In silicate melts, Al_2O_3 is known to exist in the two different forms, depending on the properties of the melt. It exists as $[AlO_4]^{5-}$ ion with 4 coordinated oxygen and forms tetrahedra network structure in basic melts, while in acid

melts it decomposes into O^{2-} and Al^{3+}, which break Si–O covalent bond as a network modifier. From the measurement result of thermal conductivity, therefore, it can be qualitatively inferred that the changes in Al_2O_3 form and role have occurred, and subsequently dependence of thermal conductivity on Al_2O_3 content has changed around Al_2O_3 15–20 mass%.

3.2. Relationship between Thermal Conductivity and Temperature and Structural Interpretation of Thermal Conductivity

Thermal conduction in silicate melts is carried out mainly by phonon vibration, and the phonon conduction in crystalline materials can be figured out by Debye's expression for thermal conductivity based on the kinetic theory of gases, as following Eq. (3).[22)]

$$\lambda = \frac{Cvl}{3} \quad \text{.....(3)}$$

Here, C, v, and l denote the heat capacity, the sound velocity, and the phonon mean free path of the sample, respectively. Also, the mean free path becomes shorter in proportion to the number of phonon increases. Therefore, thermal conductivity is considered to be inversely proportional to absolute temperature assuming heat capacity and sound velocity of silicate melt are almost constant.[23)] As a matter of fact, Nagata and Hayashi[4)] have studied the thermal conduction in simple binary silicate melts and found the linear relationship between thermal conductivity and the reciprocal of absolute temperature.

The thermal conductivities of the 30mass%CaO–18 mass%Al_2O_3–52mass%SiO_2 and 38mass%CaO–20mass% Al_2O_3–42mass%SiO_2 oxide melts were plotted versus reciprocal of the absolute temperature in **Figs. 8** and **9**. According to phonon conduction theory, the straight line which is approaching the origin at higher temperature from the full network structure was expected. The measurement results, however, show negative deviation from the linearity. Comparing Figs. 8 and 9, the negative deviation at higher temperatures becomes more remarkable with higher SiO_2 content. This disagreement can be explained by the change of network structure.

In order to consider a temperature effect on the network structure, the samples quenched from 1 673 K, 1 773 K, and 1 873 K were subjected to infrared absorption analysis. The IR absorption patterns of 30mass%CaO–18mass% Al_2O_3–52 mass%SiO_2 and 38mass%CaO–20mass%Al_2O_3–42mass%SiO_2 are shown in **Figs. 10** and **11**, respectively. Wide band appeared at the range from 1 200–800 cm^{-1}, showing the summation of IR absorptions of [SiO_4]-tetrahedra with various non-bridging oxygen per silicon

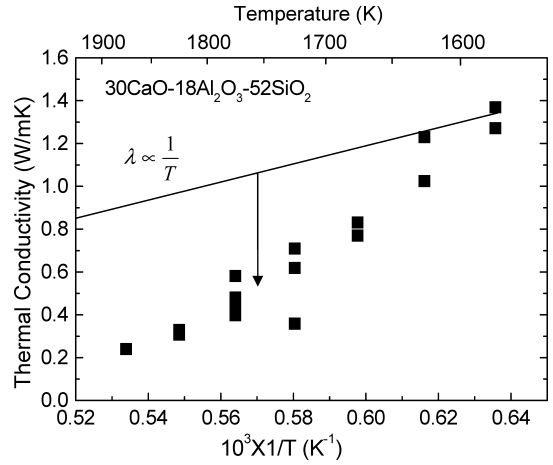

Fig. 8. Dependence of the thermal conductivity of 30mass% CaO–18mass%Al_2O_3–52mass%SiO_2 melt on the reciprocal of absolute temperature.

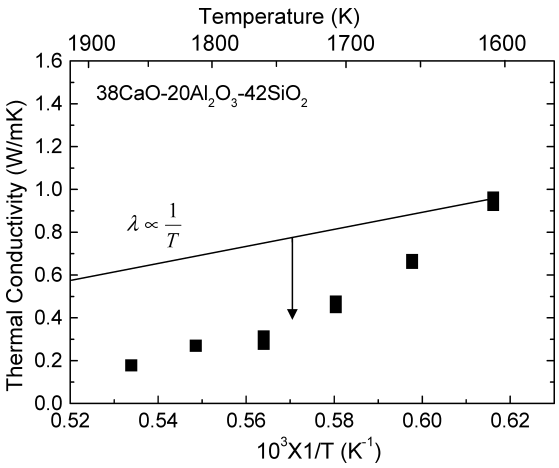

Fig. 9. Dependence of the thermal conductivity of 38mass% CaO–20mass%Al_2O_3–42mass%SiO_2 melt on the reciprocal of absolute temperature.

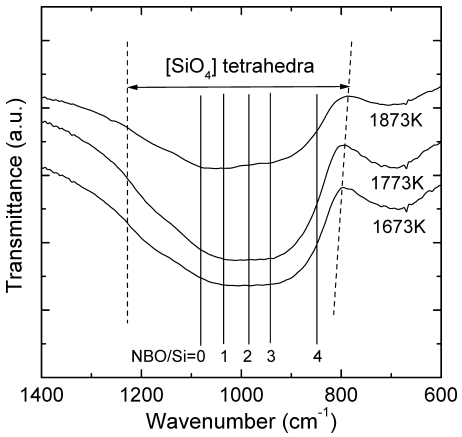

Fig. 10. IR transmittance of 30mass%CaO–18mass%Al_2O_3–52mass%SiO_2 as a function of wave number.

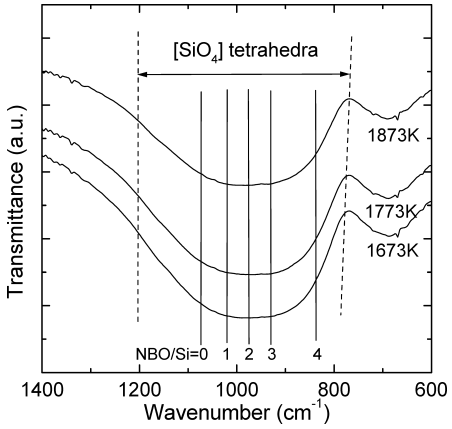

Fig. 11. IR transmittance of 38mass%CaO–20mass%Al_2O_3–40mass%SiO_2 as a function of wave number.

(NBO/Si=1, 2, 3, 4).

While IR absorptions of the samples quenched from 1 673 K and 1 773 K showed similar spectra for both compositions, that of 1 873 K demonstrated an increase in absorption at low wavenumber side of [SiO_4]-tetrahedra band, namely a shift to lower wavenumber with temperature increase. Considering that [SiO_4]-tetrahedra with NBO/Si=1, 2, 3, 4 have the specific peaks at 1 030, 980, 940 and 850 cm^{-1}, this shift can be interpreted as a depolymerisation of silicate network structure. Moreover, this was observed more significantly in case of the 30mass%CaO–18mass%Al_2O_3–52mass%SiO_2 melt compared with the 38mass%CaO–20mass%Al_2O_3–42mass%SiO_2 melt, indicating that the structure of silicate melt with higher SiO_2 content might be more sensitive to temperature.

Based on the proportional relationship between thermal conductivity and mean free path of phonon,[22] it should be noted that the mean free path may depends not only on temperature but also on the network structure changes. The mean free path is known to decrease proportionally as the absolute temperature increases in case of crystalline solid, because phonons have more chances to be scattered when the thermal vibration produces the anharmonic lattice interaction. Kittel,[24] however, predicted that the mean free path in solid glasses would be geometrically determined owing to the disorder of their structure. Since the depolymerisation takes place in the network structure of the silicate melt above the liquidus temperature, the number of thermally-broken bonds, n_{broken}, which limits the mean free path, is inversely proportional to the exponential of the reciprocal of the absolute temperature. Hence, the relationship between mean free path and the absolute temperature is obtained as Eq. (4).

$$l \propto \frac{1}{n_{\text{broken}}} \propto \exp\left(\frac{B}{RT}\right) \quad \text{.....(4)}$$

Here, R and B denote the gas constant and the apparent activation energy for bond breaking to make network pieces, respectively.

The logarithms of thermal conductivities of 30mass%CaO–18mass%Al_2O_3–52mass%SiO_2 and 38mass%CaO–20mass%Al_2O_3–42mass%SiO_2 melts were plotted *versus* $1/T$, and they show quite good linearity as shown in **Figs. 12** and **13**. Thus, thermal conductivities of these melts can be expressed by the following relationship in the present temperature range.

$$\lambda = A \exp\left(\frac{B}{RT}\right) \quad \text{.....(5)}$$

The constant A indicates the hypothetical thermal conductivity value at the infinite high temperature. These parameters were evaluated with respect to various compositions and tabulated in **Table 3**.

4. Conclusions

Thermal conductivity of the CaO–Al_2O_3–SiO_2 system was measured using non-stationary hot wire method in the range from liquidus temperature to 1 873 K. Effects of the composition and the temperature on thermal conductivity were investigated and the following conclusions were withdrawn.

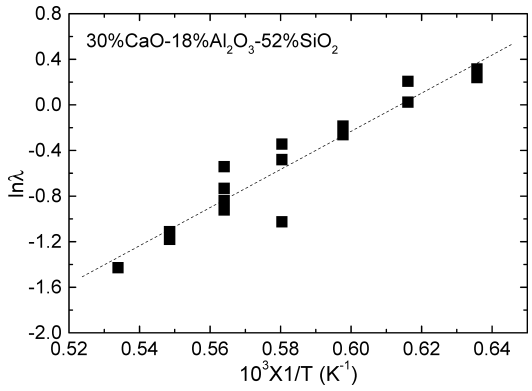

Fig. 12. Dependence of logarithm of thermal conductivity of 30mass%CaO–18mass%Al_2O_3–52mass%SiO_2 on the reciprocal of absolute temperature.

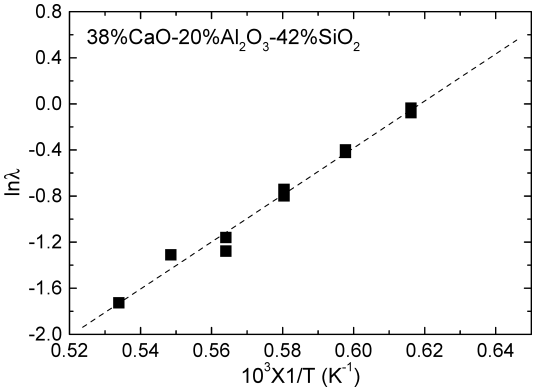

Fig. 13. Dependence of logarithm of thermal conductivity of 38mass%CaO–20mass%Al_2O_3–42mass%SiO_2 on the reciprocal of absolute temperature.

Table 3. Parameters derived from the relationship between thermal conductivity and $1/T$.

Charge composition (mass%)			$\frac{CaO}{SiO_2}$	A (W/mK)	B (kJ)	Measurement Temperature (K)
CaO	Al_2O_3	SiO_2				
26.0	8.0	66.0	0.39	7.6×10^{-7}	196	1723~1873
24.0	15.0	61.0	0.39	2.0×10^{-5}	149	1573~1873
22.0	22.0	56.0	0.39	1.7×10^{-5}	150	1673~1873
30.0	18.0	52.0	0.58	3.5×10^{-5}	139	1573~1873
38.0	20.0	42.0	0.90	3.3×10^{-6}	170	1623~1873
29.0	39.0	32.0	0.90	1.3×10^{-5}	148	1673~1873

(1) Iso-thermal conductivity contours for the CaO–Al_2O_3–SiO_2 system were drawn in the iso-thermal sections at 1 773 K, 1 823 K, and 1 873 K, respectively. Thermal conductivity decreased with increase in the ratio of CaO/SiO_2.

(2) When CaO/SiO_2=0.39 and 0.90, thermal conductivity showed the maximum value at around 15 mass% Al_2O_3, and decreased with further Al_2O_3 addition, indicating that Al_2O_3 plays a role of network former at the Al_2O_3 content lower than 15 mass%, but a network modifier at higher Al_2O_3.

(3) As for all compositions, thermal conductivity sharply decreased as temperature rises from liquidus temperature to 1 873 K. However, measured thermal conductivity showed a negative deviation from the expected linearity with the reciprocal of absolute temperature presumably due to the structure change of the silicate melts.

Acknowledgement

This research was supported by "Regional New Consortium Project for FY 2004: Development of Artificial Sea Sand Production Technology by Utilizing Blast Furnace Slag (Chugoku Bureau of Economy, Trade and Industry, Japan)". The authors are grateful to Professor M. Susa and Mr. S. Ozawa for discussion and helpful advices on the thermal conductivity measurements.

REFERENCES

1) M. Susa, K. C. Mills, M. J. Richardson, R. Taylor and D. Stewart: *Ironmaking Steelmaking*, **21** (1994), 279.
2) K. Nagata and K. S. Goto: Proc. of 2nd Int. Symp. on Metallurgical Slags and Fluxes, ed. by H. A. Fine and D. R. Gaskell, Metall. Soc. AIME, Warrendale, PA, (1984), 875.
3) K. Nagata, M. Susa and K. S. Goto: *Tetsu-to-Hagané*, **69** (1983), No. 11, 1417.
4) K. Nagata and Hayashi : *CAMP-ISIJ*, **16** (2003), 873.
5) M. Hayashi, H. Ishii, M. Susa, H. Fukuyama and K. Nagata: *Phys. Chem. Glasses,* **42** (2001), 6.
6) Nippon Slag Association: Application of Slag to Blast Furnace Slag Cement, (2003).
7) K. Nobata and Y. Ueki: *Nippon Steel Tech. Rep.*, (2002), No. 86, 44.
8) T. Mizuochi and T. Akiyama: *ISIJ Int*., **43** (2003), 1469.
9) S. Ishikuro, K. Nagata and K. S. Goto: *Trans. Iron Steel Inst. Jpn.*, **21** (1981), B-13.
10) M. Kishimoto, M. Maeda, K. Mori and Y. Kawai: Proc. of 2nd Int. Symp. on Metallurgical Slags and Fluxes, ed. by H. A. Fine and D. R. Gaskell, Metall. Soc. AIME, Warrendale, PA, (1984), 891.
11) T. Sakuraya, T. Emi, H. Ohta and Y. Waseda: *J. Jpn. Inst. Met.*, **46** (1982), 1131.
12) K. Ogino, A. Nishiwaki and K. Yamamoto: *Tetsu-to-Hagané*, **65** (1979), S683.
13) T. El Gammal and S. J. J. Sanchez de Loria: *Arch. Eisenhüttenwes.*, **39** (1986), 620.
14) A. C. Mikrovas, S. A. Argyropoulos and L. D. Sommerville: *Iron Steelmaker*, **18** (1991), No. 12, 51.
15) R. Eriksson and S. Seetharaman: *Metall. Mater. Trans. B*, **35B** (2004), 461.
16) K. C. Mills and M. Susa: *NPL Report* DMM(A) 68, "Thermal Conductivities of Slags", London, (1992), 4.
17) N. S. Srinivasan, X. G. Xiao and S. Seetharaman: *J. Appl. Phys.*, **75** (1994), 2325.
18) H. S. Carslow and J. C. Jaeger: Conduction of Heat in Solids, 2nd ed, Oxford University Press, Clarendon Inc., London, (1959), 192.
19) B. E. Warren and J. Biscoe: *J. Am. Ceram. Soc.*, **21** (1938), 259.
20) Japanese Industrial Standard Committee: JIS C1602(01), (1995), 42.
21) M. Susa, S. Kubota, M. Hayashi and K. C. Mills: *Ironmaking Steelmaking*, **28** (2001), 290.
22) P. Debye: Voträge über die kinetische Theorie der Materie und Elektruzität, ed. by B. G. Teubner, Gottinger Wolfskehlvortrage, Leipzig, and Berlin, (1914), 46.
23) K. Nagata, K. Ohira, H. Yamada and K. S. Goto: *Metall. Trans. B*, **18B** (1987), 549.
24) C. Kittel: *Phy. Rev.*, **75** (1949), 972.